Received: 8 June 2018 | Revised: 21 September 2018 | Accepted: 17 October 2018

DOI: 10.1002/mrm.27596

FULL PAPER

Magnetic Resonance in Medicine

Assessment of cardiac-driven liver movements with filtered harmonic phase image representation, optical flow quantification, and motion amplification

Stephan Hahn[1] | **Julie Absil**[2] | **Olivier Debeir**[1] | **Thierry Metens**[2]

[1]LISA - IMAGE: Laboratories of Image, Signal processing and Acoustics, Université Libre de Bruxelles, Brussels, Belgium

[2]Department of Radiology- Magnetic Resonance Imaging, Hôpital Erasme, Université Libre de Bruxelles, Brussels, Belgium

Correspondence
Stephan Hahn, LISA - IMAGE: Laboratories of Image, Signal processing and Acoustics Université Libre de Bruxelles, Brussels, Belgium CP 165/57, 50, av. Franklin Roosevelt B-1050 Bruxelles, Belgium.
Email: stephahn@ulb.ac.be
Twitter: @stephahn16

Purpose: To characterize cardiac-driven liver movements using a harmonic phase image representation (HARP) with an optical flow quantification and motion amplification method. The method was applied to define the cardiac trigger delay providing minimal signal losses in liver DWI images.

Methods: The 16-s breath-hold balanced-SSFP time resolved 20 images/s were acquired at 3T in coronal and sagittal orientations. A peripheral pulse unit signal was recorded. Cardiac-triggered DWI images were acquired after different peripheral pulse unit delays. A steerable pyramid decomposition with multiple orientations and spatial frequencies was applied. The liver motion field-map was derived from temporal variations of the HARP representation filtered around the cardiac frequency. Liver displacements were quantified with an optical flow method; moreover the right liver motion was amplified.

Results: The largest displacements were observed in the left liver (feet-head:3.70 ± 1.06 mm; anterior–posterior: 2.35 ± 0.51 mm). Displacements were statistically significantly weaker in the middle right liver (0.47 ± 0.11 mm; $P = 0.0156$). The average error was 0.013 ± 0.022 mm (coronal plane) and 0.021 ± 0.041 mm (sagittal plane). The velocity field demonstrated opposing movements of the right liver extremities during the cardiac cycle. DWI signal loss was minimized in regions and instants of smallest amplitude of both velocity and velocity gradient.

Conclusion: Cardiac-driven liver movements were quantified with combined cardiac frequency-filtered HARP and optical flow methods. A motion phase opposition between right liver extremities was demonstrated. Displacement amplitude and velocity were larger in the left liver especially along the vertical direction. Motion amplification visually emphasized cardiac-driven right liver displacements. The optimal cardiac timing minimizing signal loss in liver DWI images was derived.

KEYWORDS

cardiac cycle, diffusion imaging, harmonic phase image representation, liver, motion amplification, optical flow

1 | INTRODUCTION

The in-vivo physiological deformation of abdominal organs represents a major issue during targeted treatments (e.g., radiotherapy) and imaging. The main source of motion comes from respiration that generates a translation and a deformation of the abdominal organs.[1] However, after elimination of respiratory effects, the heart movement itself induces the propagation of a mechanical wave that mainly affects the left lobe of the liver but has some impact on other abdominal tissues too. In DWI, the cardiac movement has a nonrigid bulk motion effect that causes the signal intensity loss in the heart and in abdominal organs because of an intravoxel motion dephasing.[2]

Several studies have shown that an appropriate cardiac triggering does improve both the quality of DWI images and diffusion quantitative measurements in the left and the right lobes of the liver.[3] However, the determination of the optimum cardiac triggering remains time consuming with repeated DWI at different trigger delays[2] or rather subjective when using the visual assessment of the left liver as shown previously.[3] Furthermore, a detailed analysis of DWI images has revealed that signal attenuation due to the cardiac movement was highest in the vertical direction in the left lobe of the liver and in the left-to-right direction in the right lobe of the liver,[4] suggesting a complex propagation of the deformation wave inside the liver. Using conventional cine breath-hold MR imaging, the heart-related movements might be either detectable, especially in the left lobe of the liver, or hardly visible in other parts of the liver or in other organs.

In the liver subtle motion can be quantified by using the harmonic phase (HARP) image representation, first developed by Osman et al[5] and used for MRI tagging analysis.[6,7]

The feasibility of sub-pixel motion amplification has been demonstrated by Eulerian video magnification techniques based on the decomposition of cine time resolved images with a scaled and oriented Laplacian pyramid approach followed by temporal frequency passband filtering.[8] An alternative amplification method based on phase motion processing less prone to noise has been developed too.[9] Recently, subtle brain motions due to cardiac-induced blood pulsation have been visualized with amplified MRI (aMRI). In aMRI, motion amplification was originally performed on retrospective cardiac-gated cine images using the Eulerian approach[10] and has been then improved by the implementation of a phase-based video motion processing.[11]

The present study aims to characterize weak or imperceptible liver movements induced by the heartbeat using an HARP image representation with an optical flow quantification method and further to visually emphasize right liver displacements using a motion amplification technique. The method was applied to define the cardiac trigger delay that provides DWI images with minimal signal losses in a given region of the liver.

2 | METHODS

2.1 | Subjects

Seven healthy subjects participated in this single institution prospective study (5 males and 2 females; mean age, 31 ± 8 years). The Institutional Review Board approved this study (P2016/320 /CCB B406201628987).

2.2 | Image acquisition

All imaging experiments were performed using a 3.0T MR system (Philips Ingenia, Philips Healthcare, Best, The Netherlands). To analyze movements induced by the heart, each volunteer was dynamically imaged in coronal and sagittal planes, each acquired with a 16-s breath-hold time resolved balanced steady-state free precession (bSSFP) sequence (TR/TE/flip angle = 2.2 ms/1.1 ms/40°, matrix = 224 × 224, reconstruction voxel size = 1.75 × 1.75 mm^2, acquisition voxel size 3.65 × 3.65 × 10 mm^3, time resolution of 50 ms/frame). Each acquisition set contained 300 continuous single-slice dynamic scans, after discarding the first 25 scans to eliminate transient signal effects. A peripheral pulse unit (PPU) signal was recorded during the whole acquisition; the PPU time position corresponding to the cardiac systole was identified using coronal time resolved images. Additionally, PPU cardiac-triggered single shot spin echo-EPI DWI axial or coronal sections were acquired in a single breath-hold repeatedly after 6 different PPU delays: 300, 390, 400, 490, 500, and 590 ms (an initial dummy TR to eliminate signal transients, b = 0 s/mm^2 twice, b = 500 s/mm^2 in 3 orthogonal directions; TE = 64 ms, TR = 3 cardiac beats, 6 sections with 2 per cardiac beat, acquisition voxel size 3 × 3 × 6 mm^3, FOV 400 × 300 mm^2). The isotropic DWI image was reconstructed. For a 1-s heart period, the acquisition duration was 18 s.

2.3 | Motion measurement

2.3.1 | Overall pipeline

The objective of the image processing was to compute the motion field map12 from the bSSFP cine images.[12] The technique aims to filter the dynamic image sequence with a temporal frequency filtering to eliminate movements occurring outside the frequency of interest. More precisely, as the heartbeat is not a perfect sine function, the induced movement in the liver involves a main frequency component at the cardiac frequency and harmonics at each integer multiple of this frequency. Based on that, the frequency filters were built around the cardiac frequency and the 2 first harmonics. The filter bandwidth was set to 0.4 Hz.

This filtering was performed in the HARP image representation which is directly related to the motion field.[5,6] Based

on HARP images, an optical flow map12 was computed to quantify the displacement. Finally, a motion amplification was applied to improve the visualization of imperceptible displacements,[9] like deformations occurring in the right liver lobe (Supporting Information Video S1, which is available online).

2.3.2 | Image filtering with HARP image representation

Figure 1 illustrates the image filtering process. A steerable pyramid decomposition is applied on the bSSFP cine images on multiple orientations and spatial frequencies. The HARP images are defined as the phase part of the response to each pyramid level. The kernel filter used for the pyramid decomposition was similar to a Gabor kernel (i.e., a sinus wave under a Gaussian envelope).[9]

Then the temporal variations of the HARP images provided by the difference between consecutive time frames are filtered around the cardiac frequency and are optionally multiplied by an amplification factor α. Finally, the filtered HARP images are recombined to provide the final processed images.

If motion amplification is applied, the amplification factor α is limited to a maximum value (9). Considering the temporal bSSFP image sequence, the result of 1 pyramid level around a spatial frequency w_k and an orientation θ is:

$$I_{k,\theta}(y,t) = A_k e^{jw_k(x+\delta(t))} \quad (1)$$

where I is the pixel intensity at position y and time t, A_k represents the filter amplitude,$\delta(t)$the displacement at time t, and x the initial position coordinates. The phase part of I_k is the HARP image and is limited to the range [-π,+π). For 2 consecutive temporal frames, the difference between 2 HARP images is $w_k\delta(t)$.To avoid temporal warping, the quantity $|w_k\delta(t)|$ must be smaller than π. With an amplification factor α, it means that

$$\alpha|\delta(t)| < \frac{\pi}{w_k} = \frac{\lambda}{2} \quad (2)$$

where λ represents the spatial wavelength corresponding to the chosen spatial frequency w_k. Equation (2) means that the maximum displacement after amplification cannot be higher than the half of the chosen spatial wavelength. The amplification factor limits were computed on the basis of maximum displacements between 2 consecutives frames and spatial frequencies of the pyramid level. The amplification factors used throughout the study were always below the limits for qualitative visualization and were set to 1 (i.e., filtered and unamplified) for quantitative measurements.

2.3.3 | Motion quantification by optical flow estimation

The optical flow algorithm aims to evaluate motion between successive video frames.[13] The displacement field $\delta_t(x)$ at time t is computed as the displacement which satisfies the brightness constancy constraint equation (Equation 3).

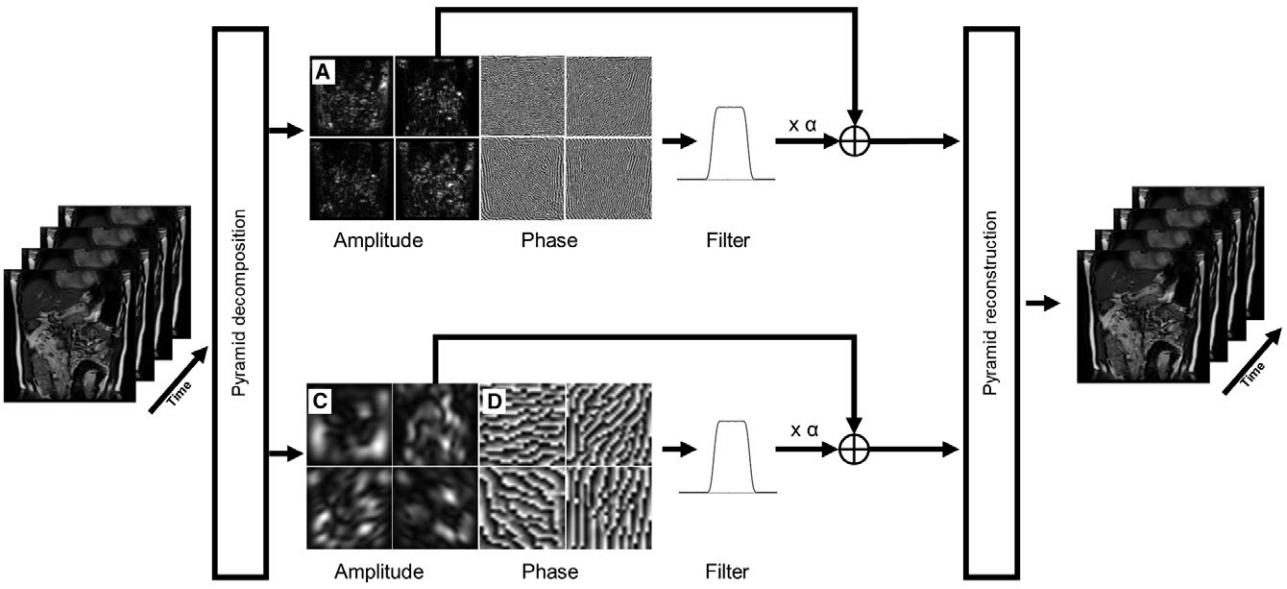

FIGURE 1 Image filtering process based on the original description by Wadhwa et al.[9] The temporal bSSFP images are decomposed using a steerable pyramid with 8 different orientations (only 4 orientations are illustrated) in multiple spatial frequencies, from coarse (C,D) to fine (A,B). The amplitudes (A–C) and the phases (HARP images) (B–D) of the filter response are computed. The temporal variations of the HARP images are filtered around the cardiac frequency and are optionally multiplied by an amplification factor α. Finally, the filtered HARP images are recombined to provide the final processed images

$$I\left(x+\delta_t(x),t+1\right)-I\left(x,t\right)=0. \quad (3)$$

The solution to Equation (3) was computed using the Farnebäck approach.[5] The overall method is based on a local polynomial expansion to smooth the image and on a coarse-to-fine solution to take into account large and small displacements. For details, see Osman et al and Fortun et al.[5,13]

One drawback of the optical flow method is the error accumulation on long video sequences.[13,14] The tracking of a point from a reference frame to the end of the sequence consists of applying successively each motion field computed between consecutive frames, leading to a nonnull total drift error. To deal with this constraint, it was hypothesized that the global maximum displacement remained relatively small and all displacements were cyclical. From these hypotheses, the optical flow was computed as

$$I\left(x+\delta_{ref-t}(x),t\right)-I\left(x,ref\right)=0 \quad (4)$$

in which *ref* represents a reference frame and the displacement between this reference frame and the frame at a temporal position *t*. However, the choice of an arbitrary reference frame has an impact on the resulting motion field. More precisely, during the acquisition, 2 kinds of variation can occur. One cardiac cycle can be affected by time-localized macroscopic movement (e.g., involuntary breathing during a short time slot) and inside a cardiac cycle, large partial volume effects can occur, i.e., part of a tissue might leave and reenter the slice volume. Ideally, the optical flow measurement must be independent of the temporal location of this reference frame. Thereby the final motion field was computed as the mean value of motion fields calculated from multiple reference frames. The reference frames are randomly picked using a uniform distribution of the acquired bSSFP images composed of ~15 heartbeats of ~20 frames duration. This motion field is at a subpixel resolution.

The quantification method described above was validated on a simulated phantom (see the Appendix).

2.4 | Measurements

The obtained motion field was computed using the unamplified, temporally filtered bSSFP images. A mean cardiac cycle motion field was constructed as the mean value across all cardiac cycles. 2D color coded velocity vector maps were constructed.

The common error evaluation of the optical flow is based on 2 measurements: the endpoint error (EE) and the angular error (AE).[15] The EE is an Euclidian distance between the real and the computed location of a tracked point. The AE is an angular distance between the real orientation and the last computed orientation of the displacement vector. Because of the lack of ground truth values for the optical flow method, it was not possible to measure the real AE and EE. However, the EE was evaluated under the cyclical hypothesis: for a given point of interest (POI) in the liver, the starting point and the end point must be spatially close considering a time slot of 1 mean cardiac cycle.

For quantitative measurements of displacements, the trajectory of the POI in the imaging plane was computed and the velocity was calculated across the mean cardiac cycle. The maximum displacement was calculated in the feet–head (FH) direction in 4 locations (left liver in Couinaud segment 2; right liver: dome, center, and bottom) and in the anterior–posterior (AP) direction in a left liver region close to the aorta.

To identify pixels with imperceptible movements related to cardiac motion, the standard deviation of the temporal signal intensity was calculated in each pixel and a standard deviation map was obtained in the right liver lobe, without and after amplification.

A visual inspection of DWI images acquired with different PPU cardiac trigger delays was performed to identify the PPU trigger delay providing images with the lowest signal attenuation. This delay was compared with a trigger time computed from the motion velocity field that corresponded to the minimum displacement. Our hypothesis was to consider the latter to be the best candidate for optimal diffusion-weighted cardiac triggering.[3] From the motion velocity field, the time interval with minimum movement was also computed.

2.5 | Statistics

The statistical analyses were performed using MedCalc Statistical Software version 17.6 (MedCalc Software bvba, Ostend, Belgium). The nonparametric Wilcoxon signed-rank test was performed to compare the different maximum displacements in the liver and to compare visual diffusion-weighted trigger delays with motion field minimum displacement trigger times. The correlation between cardiac frequency and minimum displacement time interval was assessed using Pearson correlation coefficient. A P value < 0.05 was considered as significant.

3 | RESULTS

3.1 | Optical flow method

Figure 2 illustrates optical flow measurements. The POI was taken in the left liver lobe (in Couinaud segment 2) just under the heart. For this point, the trajectory in the imaging plane and the velocity in right–left (RL) and FH axes were plotted. On RL axis, positive and negative velocity values, respectively, mean movement toward the left and right directions and on FH axis, positive and negative velocity values, respectively, mean

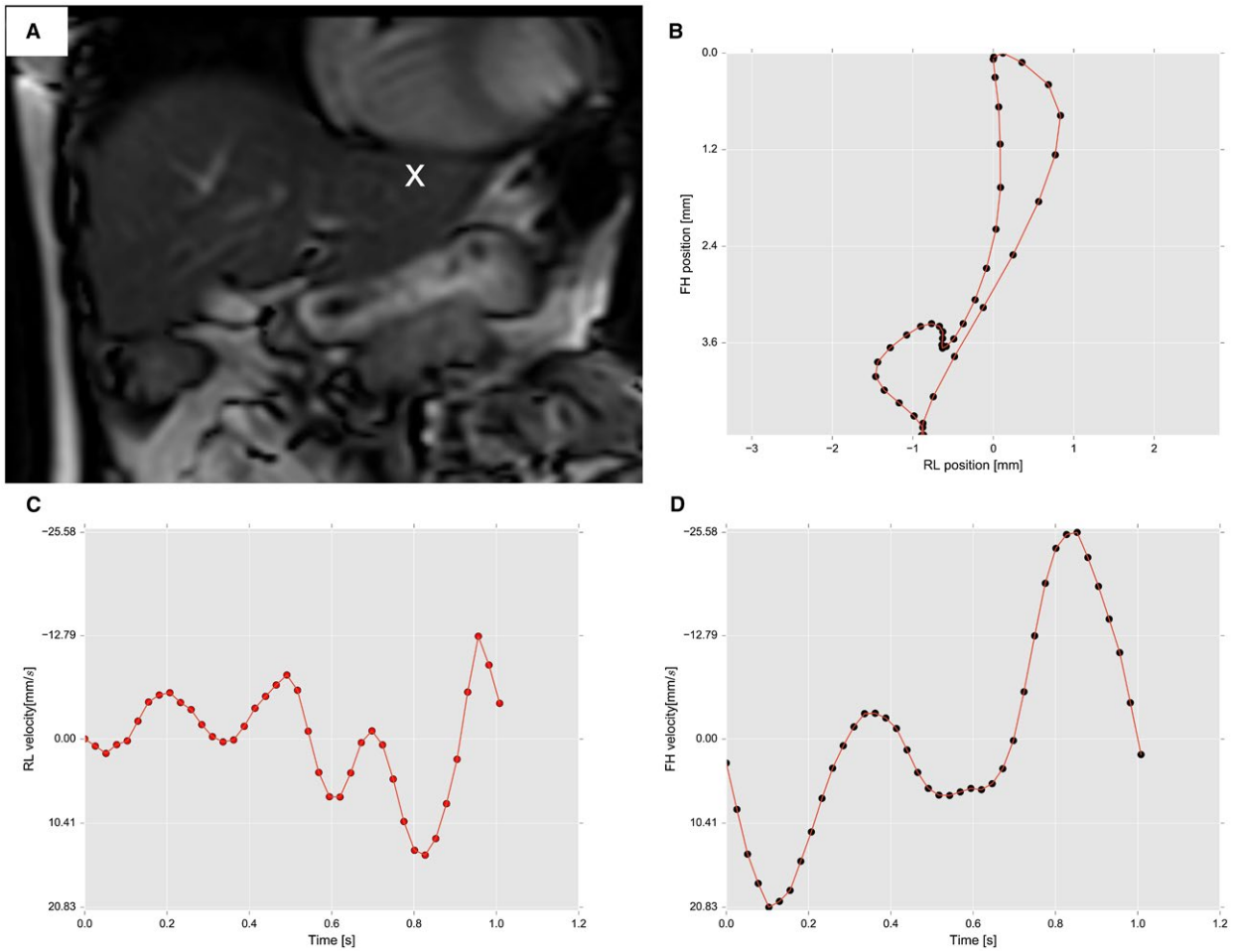

FIGURE 2 A, bSSFP image with the POI marked in white. B, POI trajectory during the mean cardiac cycle. The final point position is very close to the initial one. C–D, POI velocity along the time, respectively, in RL and FH directions. C, Negative values mean that the POI is moving toward the right. D, Negative values mean that the POI is moving in the cranial direction (systolic phase). Note that FH velocities and displacements are higher than in the RL direction

movement toward the caudal and cranial directions. The average EE measured on the liver was 0.013 ± 0.022 mm in the coronal plane and 0.021 ± 0.041 mm in the sagittal plane. FH velocities and displacements were higher than in the RL direction.

The heartbeat phases are recognizable on the FH velocity graph taken just under the heart. Indeed, during the diastolic phase the left liver lobe undergoes a caudal displacement while during systolic phase the displacement is cranial.

Table 1 provides a summary of maximum displacements in mm observed in 5 different liver regions (left liver lobe under the heart in Couinaud segment 2 and close to the aorta; right liver: close to the dome, at the center, and at the bottom).

In the left liver lobe, the displacements were measured just under the heart (Couinaud segment 2) in the coronal plane in the FH direction and near the aorta in the sagittal plane in the AP direction. In the right lobe, the displacements were measured in the FH direction. The largest displacements induced by the heart movement are observed in the left liver lobe, in the FH direction. In the AP direction, the aorta is also a source of motion in the left lobe. In the right lobe, the displacements are weaker than elsewhere.

3.2 | Motion amplification in the right liver

As observed in Table 1, the total cardiac induced displacement in the right liver lobe across the whole cardiac cycle was smaller than 1 mm. It means that the displacement from 1 temporal frame to the next one is imperceptible at the image resolution. An amplification factor ($\alpha = 20$) was applied to the right liver lobe to emphasize the periodic movements close to the cardiac frequency as illustrated by a temporal standard deviation map (Figure 3 and see Supporting Information Video S2). The nonperiodic intestinal peristalsis is attenuated in amplified images, while immobile regions are not affected by the amplification process.

TABLE 1 Statistics of the maximum displacements in millimeters[a]

Subject	Left liver	Right liver dome	Right liver middle	Right liver bottom	AP left liver aorta
VOL01	4.9	0.51	0.54	0.25	1.96
VOL02	4.56	0.75	0.32	0.32	1.44
VOL03	2.71	0.61	0.39	0.52	2.6
VOL04	2.84	0.85	0.36	0.36	2.68
VOL05	4.03	0.89	0.53	1.05	2.91
VOL06	2.3	0.94	0.59	0.72	2.25
VOL07	4.6	0.94	0.54	0.32	2.62
Mean	3.7	0.78	0.47	0.50	2.35
SD	1.06	0.17	0.11	0.29	0.51
P-Value (comparison with left liver)	…	**0.0156**	**0.0156**	**0.0156**	**0.0156**
P-Value (comparison with right dome)	…	**…**	**0.0313**	**0.0469**	**…**
P-Value (comparison with right middle)	…	…	…	1.0	…

Abbreviations: AP, anterior–posterior; VOL, volunteer.
Bold *P*-values are statistically significant.
[a]*P*-Values quoted are for the Wilcoxon signed-rank test.

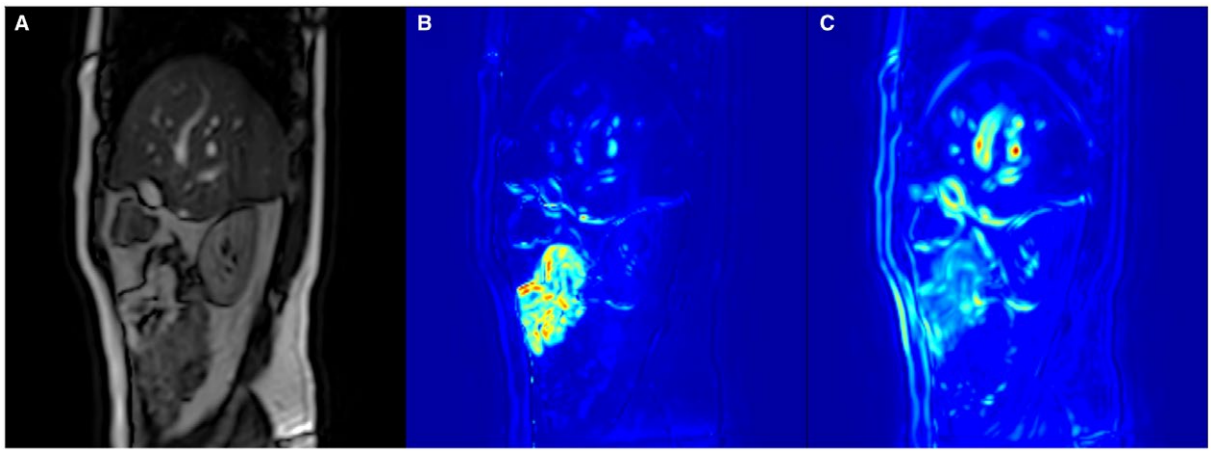

FIGURE 3 Standard deviation map of temporal pixel intensities in the right liver lobe. A, Sagittal bSSFP image at t = 0. B,C, Temporal standard deviations, respectively, without and with a 20× motion amplification, color coded from blue to red corresponding to an increasing temporal signal standard deviation. The amplification emphasizes a periodic movement close to the cardiac frequency (liver, skin, kidney). In contrast the nonperiodic intestinal peristalsis is attenuated in amplified images. Immobile regions are not affected by the amplification process. As the pixel intensities of tissues are very homogeneous, only moving borders are visible on standard deviation maps

3.3 | Motion impact on DWI images

Table 2 compares the best visual PPU trigger delay and the trigger time computed from the motion field analysis ($P = 0.11$) and gives the minimum displacement time interval. The latter was inversely proportional to the cardiac frequency ($R = -0.7641$; $P = 0.0455$).

Figure 4 illustrates liver coronal DWI images acquired with different PPU trigger delays and corresponding 2D color coded velocity maps, together with a graph of a POI velocity along the cardiac cycle.

The cardiac-related signal loss artifact in the left liver lobe was minimum when images were acquired after a trigger delay corresponding to the time interval with minimum velocity and minimum local velocity gradients.

3.4 | Velocity wave propagation

Figure 5 displays 2D color coded velocity maps computed during the diastolic and systolic phases in the right and left liver lobes. Systolic liver velocities were larger than diastolic ones. The top and bottom of the right liver lobe move in opposite directions during both cardiac phases, while the center of the right lobe moves less. The cardiac induced movement is also transmitted through the aorta and the inferior vena cava: the main contribution of the aorta is in the AP direction

TABLE 2 Best PPU cardiac trigger delay for diffusion-weighted acquisition compared to minimum displacement trigger delay[a]

Subject	Heartbeat (BPM)	Best diffusion-weighted visual trigger delay [ms]	Minimum displacement trigger delay [ms]	Minimum displacement time interval [ms]
VOL01	60	300	269	443
VOL02	58.2	280	284	249
VOL03	96	400	330	111
VOL04	89.4	500	488	69
VOL05	78.6	300	248	157
VOL06	67.2	300	315	160
VOL07	80.4	500	230	85

Abbreviations: BPM, beats per minute; PPU, peripheral pulse unit; VOL, volunteer.

[a]The best timing was visually assessed on DWI images. From the motion velocity field, the trigger time corresponding to the minimum movement and the time interval with minimum movement were computed: the latter, as expected, appears to be inversely proportional to the heart frequency.

in the left lobe while the contribution transmitted by means of the inferior vena cava is in the RL direction in the right lobe.

4 | DISCUSSION

Our study deals with the detection and quantification of small cardiac-related movements in the liver by combining frequency filtering around the cardiac frequency and an optical flow technique, altogether applied to images from a short breath-hold time resolved sequence. Motion amplification was selectively performed in the right liver to enable the visualization of otherwise invisible movements. The method provided consistent results as the initial and the integrated final positions in the cardiac cycle remained very close after processing.

As expected, movements had a larger amplitude in the left lobe of the liver close to the heart. However, motion of lower amplitude was also detected in the AP and LR directions and we evidenced regions of the liver where the movement was transmitted by means of the aorta and passively by means of the vena cava. Indeed motion amplification enabled us to visually characterize imperceptible movements in the right liver. To our knowledge, it is the first time that these deformations were illustrated. This method allows a better understanding of how normal organ shape changes under imperceptible displacements. In principle, our method is also applicable to the spleen, the pancreas and the kidneys.

Several other studies[16-19] investigated liver movements by using a different approach based on MR tagging images further processed with Gabor filters and harmonic phase analysis to track the deformation of MR tags, the available time resolution was also close to 50 ms. In healthy subjects the displacement observed by Chung et al[16] in the left liver lobe was approximately 3.5 mm, similarly to our results. However, in the right liver lobe, they identified little or no displacement. Harouni et al[19] used fast strain-encoded imaging at 3T which measures a left liver lobe strain, directly defined as the percentage change in length of the tissue compared with the tissue initial length before deformation. Sprengers et al[17] studied bowel motion patterns in the abdomen by means of a continuous tagging, while Watanabe et al[18] used tagging to evaluate the bending energy in patients with liver fibrosis.

These tagging methods were, however, not very sensitive to very small displacements, in contrast our approach did not deal with liver elastography and no strain maps were presented, but was able to detect and analyze very small movements in the right liver with motion amplification

Interestingly, at a given location in the liver, we applied our method to detect the time interval inside the cardiac cycle for which the displacement is minimum (lowest amplitude, lowest velocity and acceleration). The minimum displacement trigger delay found with this approach matched the delay for which the DWI images were less affected by the cardiac-related signal loss. This method is actually less subjective than a visual assessment of the left liver lobe displacement as suggested before,[3] that moreover could not be used for the right liver or the pancreas. In contrast, the new method is applicable to any region of the liver and probably to other organs as well.

More globally, the analysis of the motion velocity field revealed that the cardiac-related signal loss manifested mostly in regions and instants where the amplitude of both velocity and velocity gradient were pronounced. This result consists of an indirect validation of the present approach, but at the same time contributes to the understanding of cardiac-related DWI signal losses in the liver.

Our analysis also revealed a phase opposition in the movement of the right liver extremities, which might be related to the elasticity of this organ. Motion amplification allowed the direct visualization of this peculiar feature. As no patient was included, we could not verify the effect of liver fibrosis on this phase opposition. Furthermore, in addition to the direct propagation of the heart movement, a possible indirect contribution from the aorta and large blood vessels may influence the induced complete movement.

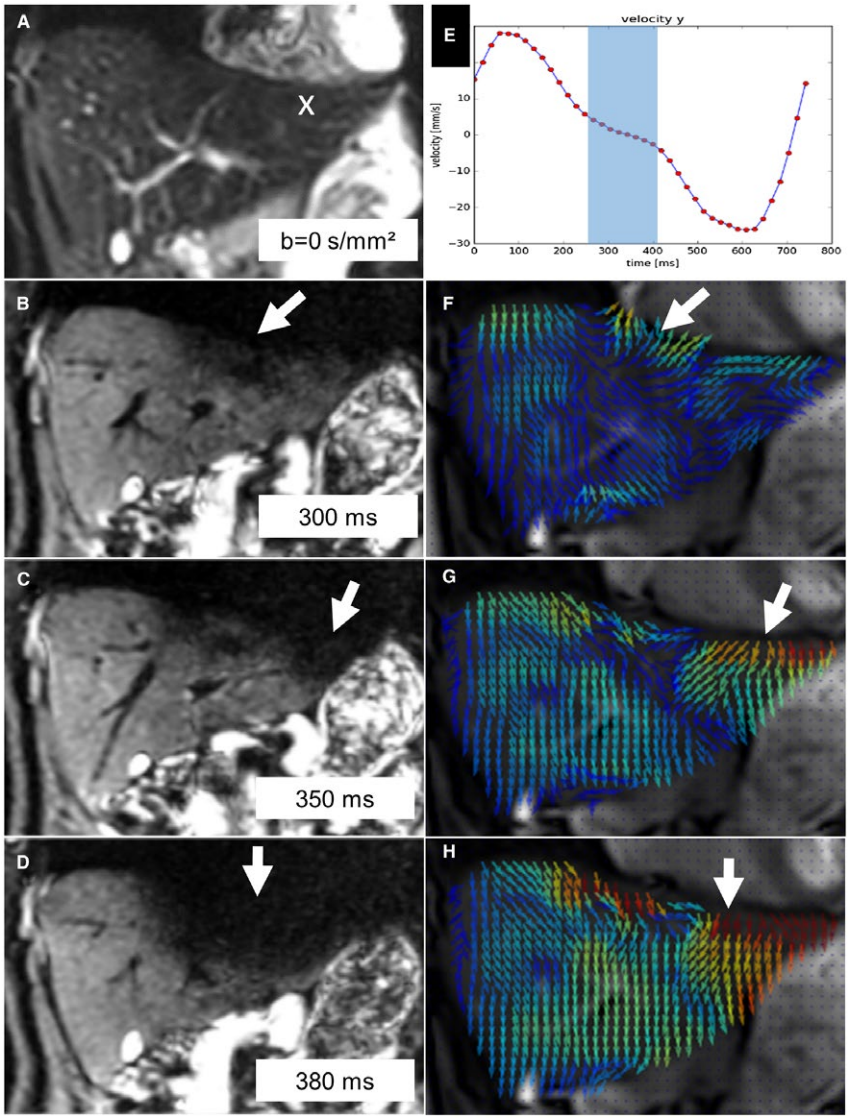

FIGURE 4 Liver coronal DWI images acquired at a fixed position with different PPU trigger delays in Vol 05. A, b = 0 image with a POI located in the liver left lobe beneath the heart (Couinaud segment 2), indicated by a cross. B–D, b = 500 s/mm^2 images at, respectively, 300, 350, and 380 ms. F–H, The corresponding 2D color coded velocity maps (increasing amplitude from blue to red). The amplitude of the cardiac-related artifact (white arrows) in the left liver lobe depends on the cardiac triggering time and visually correlates with the distribution and the amplitude of the velocities: signal void locations correspond to largest velocities and largest velocity gradients. E, POI velocity along the time in the FH direction. The minimum velocity time interval (blue overlay) starts at 248 ms and ends at 405 ms. For a diffusion acquisition duration of 80 ms, the acquisition must be started between 300 and 325 ms to avoid large velocity gradients that might result in strong signal losses

Prior studies by Holdsworth et al and Terem et al[10,11] dealt with frequency selective Eulerian movement amplification in the brain. Similarly to our results, very small movements were detected using motion amplification, based on Laplacian pyramid[10] or steerable pyramid.[11] The phase amplification used here and in Terem et al[11] allows larger amplification factors and generates less noise compared with the original Eulerian amplification.[9,10]

This study presents some limitations. These are linked to the drawbacks of the optical flow method, i.e., a boundary is needed between tissues of different intensity to enable the displacement evaluation. The liver appears to be a good candidate for this method, because numerous vein or bile duct sections demonstrate a high contrast with the liver parenchyma in bSSFP T2/T1-weighted images. Note that we discarded images obtained during the first seconds of the acquisition to allow the spin system to reach a steady state signal, otherwise transient signal variations would interfere with the displacement detection. The spatial resolution was also limited, essentially because a smaller pixel size would lead to a SNR penalty and so would affect the quality of the results.

As we did not test the method in patients with liver fibrosis or cirrhosis, we cannot predict whether fibrosis information can be obtained on the basis of our approach, further clinical investigation should be undertaken.

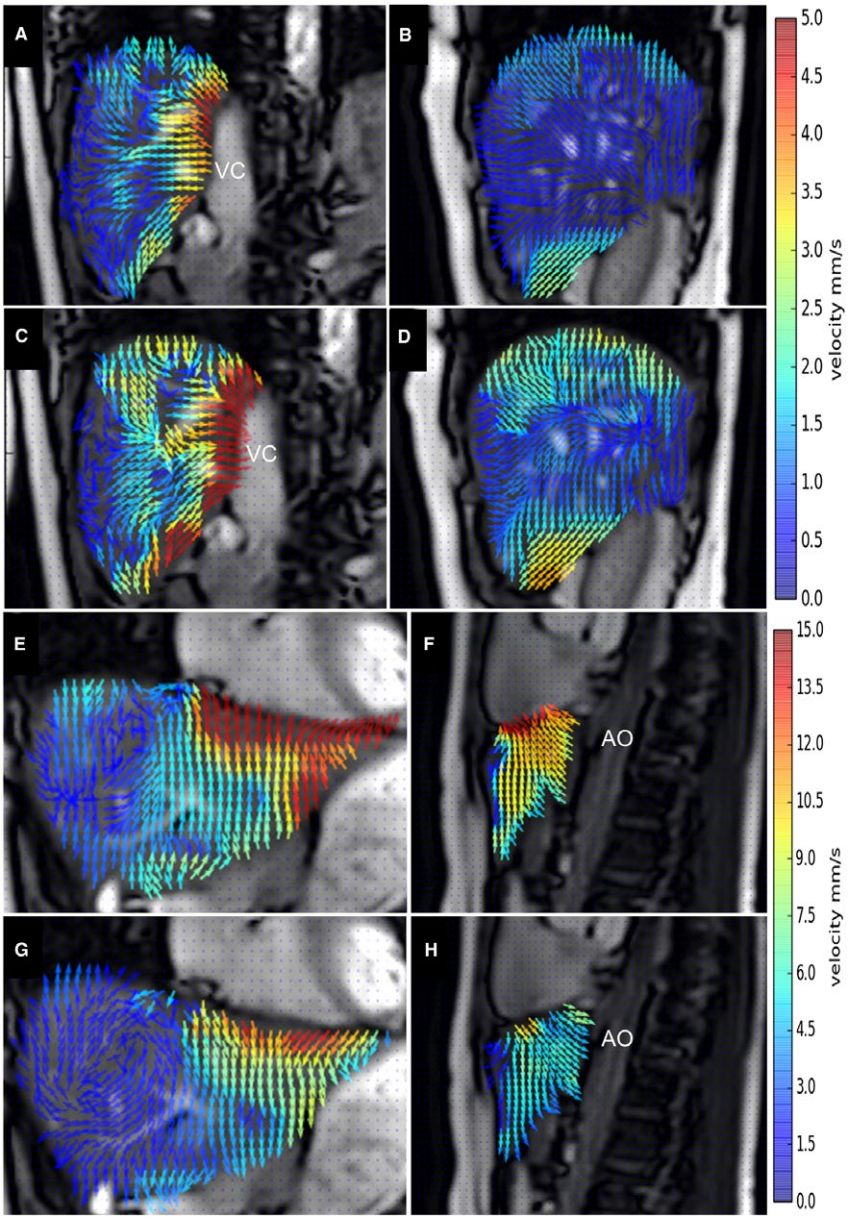

FIGURE 5 2D color coded velocity maps computed in the right (top) and left liver (bottom) lobes during the diastolic (A,B,E,F) and systolic phases (C,D,G,H) in the coronal (A,C,E,G) and the sagittal (B,D,F,H) planes. The color represents an increasing velocity range from blue to red. Note that the velocity range was modified for the left liver lobe images to avoid a color saturation. Generally, at the systolic phase the liver velocities are larger than at the diastolic phase. The pressure applied by the heart propagates mainly in the FH direction but is transmitted into the right liver lobe in the RL (A,C) and AP directions (B,D) too. The top and bottom of the right liver lobe are moving in opposite directions during both cardiac phases, while the center of the right lobe moves less. The aorta and the inferior vena cava (VC) apply a pressure on the liver during the systolic and the diastolic phases. The main contribution of the aorta is in the AP direction in the left lobe (F–H), while the contribution transmitted by means of the inferior vena cava is in the RL direction in the right lobe (A–C)

We used a breath hold acquisition to eliminate the effects of the respiratory movement together with PPU signal measurements. Ideally, both respiratory and ECG cardiac triggering should be performed, however, at the cost of much longer acquisition times.

In conclusion, we presented a method based on HARP image representation with an optical flow method to quantify cardiac-related liver displacements. The algorithm was further combined with motion amplification to display small abdominal movements linked to the cardiac movement. As expected, the amplitude of the displacement field and its associated velocity were most prominent in left liver lobe especially in the vertical direction, while movement characteristics were detected in the right liver lobe, suggesting a phase opposition between its extremities. The method was successfully applied to define the cardiac trigger delay that provides DWI with minimum signal losses in a given region of the liver.

ORCID

Stephan Hahn https://orcid.org/0000-0002-7847-6688

REFERENCES

1. Bussels B, Goethals L, Feron M, et al. Respiration-induced movement of the upper abdominal organs: a pitfall for the three-dimensional conformal radiation treatment of pancreatic cancer. *Radiother Oncol*. 2003;68:69–74.
2. Mürtz P, Flacke S, Träber F, van den Brink JS, Gieseke J, Schild HH. Abdomen: diffusion-weighted MR imaging with pulse-triggered single-shot sequences. *Radiology*. 2002;224:258–264.
3. Metens T, Absil J, Denolin V, Bali MA, Matos C. Liver apparent diffusion coefficient repeatability with individually predetermined optimal cardiac timing and artifact elimination by signal filtering. *J Magn Reson Imaging*. 2016;43:1100–1110.
4. Kwee TC, Takahara T, Niwa T, et al. Influence of cardiac motion on diffusion-weighted magnetic resonance imaging of the liver. *MAGMA*. 2009;22:319–325.
5. Osman NF, Kerwin WS, McVeigh ER, Prince JL. Cardiac motion tracking using CINE harmonic phase (HARP) magnetic resonance imaging. *Magn Reson Med*. 1999;42:1048–1060.
6. Liu W, Chen J, Ji S, et al. HARP MRI Tagging for direct quantification of Lagrangian strain in rat hearts after myocardial infarction. *J Biomech Eng*. 2004;126:523–528.
7. Monti S, Palma G, Ragucci M, Mannelli L, Mancini M, Prinster A. Optimization of tagged MRI for Quantification of liver stiffness using computer simulated data. *PLoS ONE*. 2014;9:e111852.
8. Wu H, Rubinstein M, Shih E, Guttag J, Durand F, Freeman WT. Eulerian video magnification for revealing subtle changes in the world. *ACM Trans Graph*. 2012;31:4.
9. Wadhwa N, Rubinstein M, Durand F, Freeman WT. Phase-based video motion processing. *ACM Trans Graph*. 2013;32.
10. Holdsworth SJ, Rahimi MS, Ni WW, Zaharchuk G, Moseley ME. Amplified magnetic resonance imaging (aMRI). *Magn Reson Med*. 2016;75:2245–2254.
11. Terem I, Ni WW, Goubran M, et al. Revealing sub-voxel motions of brain tissue using phase-based amplified MRI (aMRI). *Magn Reson Med*. 2018;80:2549–2559.
12. Farnebäck G. Two-frame motion estimation based on polynomial expansion. In: *Analysis. Lecture Notes in Computer Science*. Berlin, Heidelberg: Springer; 2003:363–370.
13. Fortun D, Bouthemy P, Kervrann C. Optical flow modeling and computation: a survey. *Comput Vis Image Underst*. 2015;134:1–21.
14. Li W, Cosker D, Brown M. Drift robust non-rigid optical flow enhancement for long sequences. *ArXiv160302252 Cs [Internet]*. 2016. https://arxiv.org/abs/1603.02252.
15. Baker S, Scharstein D, Lewis JP, Roth S, Black MJ, Szeliski R. A database and evaluation methodology for optical flow. *Int J Comput Vis*. 2011;92:1–31.
16. Chung S, Breton E, Mannelli L, Axel L. Liver stiffness assessment by tagged MRI of cardiac-induced liver motion. *Magn Reson Med*. 2011;65:949–955.
17. Sprengers A, van der Paardt MP, Zijta FM, et al. Use of continuously MR tagged imaging for automated motion assessment in the abdomen: A feasibility study. *J Magn Reson Imaging*. 2012;36:492–497.
18. Watanabe H, Kanematsu M, Kitagawa T, et al. MR elastography of the liver at 3 T with cine-tagging and bending energy analysis: preliminary results. *Eur Radiol*. 2010;20:2381–2389.
19. Harouni AA, Gharib AM, Osman NF, Morse C, Heller T, Abd-Elmoniem KZ. Assessment of liver fibrosis using fast strain-encoded MRI driven by inherent cardiac motion. *Magn Reson Med*. 2015;74:106–114.

SUPPORTING INFORMATION

Additional supporting information may be found online in the Supporting Information section at the end of the article.

VIDEO S1 From left to right: the original unamplified bSSFP cine images of the right liver (sagittal plane), the 20× motion amplified images around, respectively, 1 Hz, 2 Hz, and 3 Hz. The cardiac influence consists of a fundamental component at the cardiac frequency (1Hz for this volunteer) but also of harmonics (integer multiples of the fundamental frequency). Of interest, movements in AP and FH directions are depicted on the principal frequency (1 Hz), while the movements in AP direction are much less visible on the harmonic images (2 and 3 Hz).

VIDEO S2 From left to right: the original unamplified bSSFP and the 20× motion amplified around 1Hz to 3Hz. Despite the distance between the heart and the right liver, the cardiac motion still induces some degree of right liver deformation, as highlighted by the motion amplification.

How to cite this article: Hahn S, Absil J, Debeir O, Metens T. Assessment of cardiac-driven liver movements with filtered harmonic phase image representation, optical flow quantification, and motion amplification. *Magn. Reson. Med.*. 2018;00:1–11. https://doi.org/10.1002/mrm.27596

APPENDIX A

To validate the displacements measured by our method, a dynamic numerical phantom was designed. The phantom was a smoothed disk, moving from left to right, following a known sine wave displacement. The sine wave was simulated with a frequency from 1 to 3 Hz, and several combinations of these frequencies. Our quantification method was applied, and the measurements at the disk center were compared with the real displacement. In all experiments, our method succeeded to measure the displacement, with an accuracy of 98%. Figure A1 illustrates an example of the simulation for a combination of frequencies from 1 to 3 Hz.

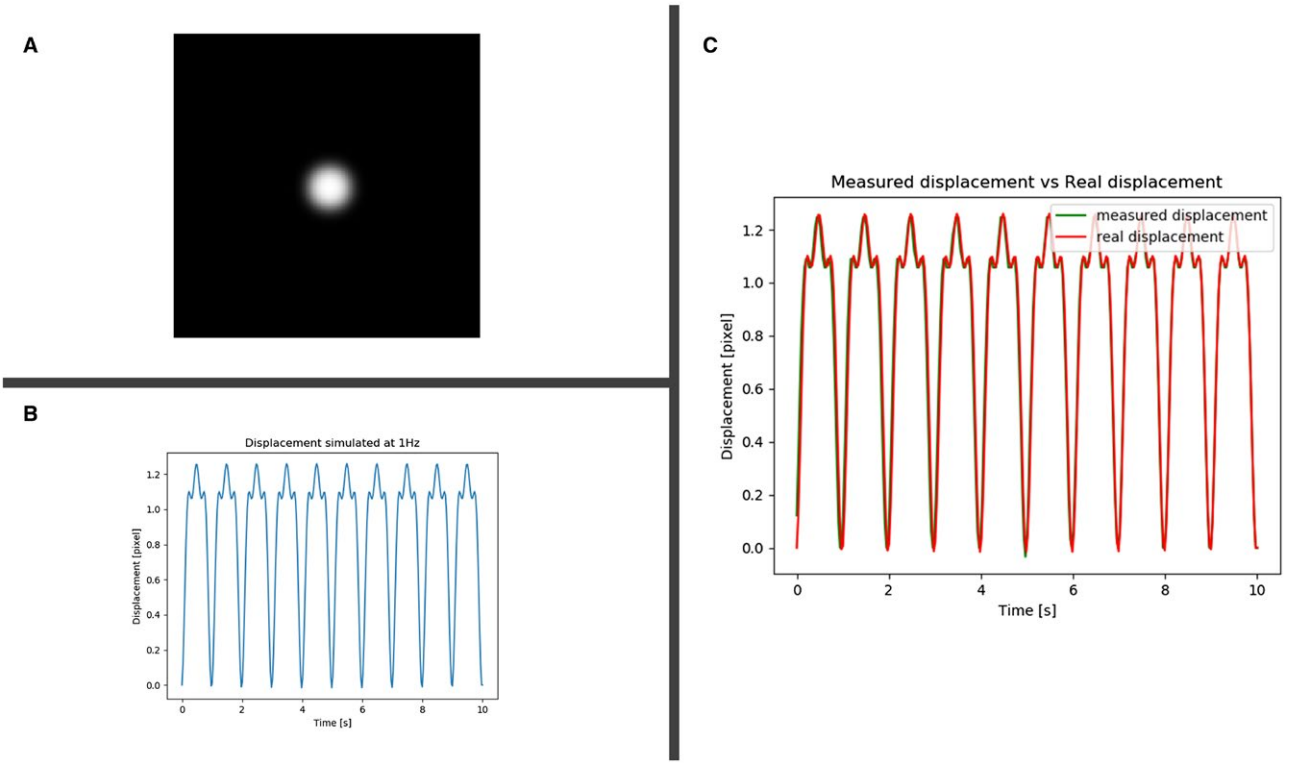

FIGURE A1 A, The virtual numerical phantom consists in a smoothed disk moving with a known displacement sine wave. B, Example of the sine wave composed of frequencies from 1 to 3 Hz. C, The measured displacement of the disk center matches the real displacement